Measurement 151 (2020) 107182

Contents lists available at ScienceDirect

Measurement

journal homepage: www.elsevier.com/locate/measurement

Battery prognostics at different operating conditions

Dong Wang [a], Jin-zhen Kong [a], Fangfang Yang [b], Yang Zhao [b,*], Kwok-Leung Tsui [b]

[a] The State Key Laboratory of Mechanical Systems and Vibration, Shanghai Jiao Tong University, Shanghai 200240, PR China
[b] School of Data Science, City University of Hong Kong, Hong Kong, China

ARTICLE INFO

Article history:
Received 29 March 2019
Received in revised form 2 September 2019
Accepted 19 October 2019
Available online 25 October 2019

Keywords:
Battery management systems
Bayesian methods
Lithium batteries
Prognostics and health management
Remaining life assessment

ABSTRACT

Rechargeable batteries become one of the most popular energy storage devices. For battery state of health prediction, discharge rate and temperature are two crucial factors that significantly affect battery discharge capacity fade. Battery discharge capacity fade modeling at different operating conditions is still an ongoing research direction. In this paper, two new battery discharge capacity fade models are proposed. In the first model, a relationship between capacity fading and discharge rate is formulated. The second model derives a relation between capacity fading and temperature. Then, two Bayesian updating procedures are respectively designed to model a unit-to-unit capacity fade variance and incorporate on-line data of a single operating battery into the two battery fade models. At last, two case studies are provided to illustrate how the proposed two discharge capacity fade models work. Results show that the proposed two new models can accurately predict battery state of health at different discharge rates and different temperatures.

1. Introduction

Lithium-ion batteries become one of the most useful energy storage devices and they have been widely used in hybrid electric vehicles, portable electronic devices, etc [1]. When batteries are charged and discharged over time, their discharge capacity fades. To provide continuous and reliable electric power sources for the aforementioned systems and devices, battery prognostics and health management [2] is required. Rich literature [3] can be found to characterize battery health status including state of charge and state of health. State of charge is a short-term parameter to indicate remaining energy at a given charge–discharge cycle. State of health is a long-term parameter to indicate remaining charge–discharge cycles, namely remaining useful life (RUL) [4,5]. Because these two basic battery parameters can not be directly measured, they are estimated and predicted by using other collected measurements, such as current, voltage, temperature, etc.

In the past years, many state of charge estimation models [6–8] have been proposed and they can work at different operating conditions, such as different discharge rates and different temperatures. Wei et al. [9] proposed a state of charge estimation method based on a recursive total least squares-based observer, which is able to accurately estimate battery state of charge. Ali et al. [10] used the Lagrange multiplier method to adaptively estimate battery state of charge and achieved high prediction accuracies. Liu et al. [11] proposed a partial adaptive forgetting factor least square method to estimate deep-discharging lithium-ion battery state of charge. However, most battery state of health prediction models [12] solely consider constant operating conditions, such as a fixed discharge rate and a room temperature. Saha et al. [13,14] proposed using an equivalent electric circuit model with an exponential form to model battery capacity fade and then employed the combination of relevance vector machines and several particle filters to predict battery RUL. Following this pioneer work, many battery prognostic methods have been reported. He et al. [15] proposed using an bi-exponential fade model instead of an exponential fade model to achieve a better regression ability for fitting battery capacity fade and then employed a particle filter to estimate the posterior parameters of the bi-exponential model and extrapolate the determined model to a failure threshold, such as 80 percent of an initial capacity, for battery RUL prediction. Xing et al. [16] proposed the integration of an exponential model and a polynomial model with an order of 2 to improve the local fitting ability of the bi-exponential model and then used a particle filter to posteriorly update model parameters for on-line battery RUL prediction. Yang et al. [17] developed a two-term logarithmic model to capture two-phase battery degradation and predict battery RUL using a particle filter. Yu et al. [18] proposed a probabilistic health indicator based state space model and used a particle

* Corresponding author.
E-mail addresses: dongwang4-c@sjtu.edu.cn (D. Wang), kongjinzhen@sjtu.edu.cn (J.-z. Kong), fangfyang2-c@my.cityu.edu.hk (F. Yang), yang.zhao@my.cityu.edu.hk (Y. Zhao), kltsui@cityu.edu.hk (K.-L. Tsui).

https://doi.org/10.1016/j.measurement.2019.107182
0263-2241/

filter to update model parameters for battery prognostics. Miao et al. [19] used an unscented Kalman filter to provide an importance function for the use of a particle filter for battery prognostics. Other candidates for the unscented Kalman filter used in the unscented Kalman filter include a Gauss–Hermite Kalman filter [20], a spherical cubature Kalman filter [21], etc.. More variants of particle filters and their applications to battery prognostics can be found in [22]. Xu et al. [23] proposed a hierarchical battery fade model and used Gibbs sampling for battery prognostics. Olivares et al. [24] found that capacity increments caused by capacity regeneration phenomena have influence on battery prognostics. In their battery state space modeling, they took detection of capacity regeneration phenomena into consideration. Zhang et al. [25] proposed a stochastic battery model with state recovery to predict battery RUL in the case of capacity regeneration phenomena. Liu et al. [26] considered the unification of battery capacity and time interval of equal discharging voltage difference series and then proposed an integrated probabilistic approach to predict battery RUL. Si [27] proposed an adaptive Brownian motion based battery prognostic method, the parameters of which were posteriorly updated by on-line data. Then, the first hitting time of the Brownian motion was used to predict battery RUL. Wang and Tsui [28] discovered a commonly underlying assumption used in the state space modeling of Brownian motion and proposed a new state space model to adaptively update model parameters. Then, they applied the new model to predict battery state of health.

The aforementioned studies assumed that rechargeable batteries work at fixed operating conditions. Operating conditions including discharge rate and temperature have significant influence on battery discharge capacity and its fade [29]. For example, a battery operating at a higher temperature fades faster than that operating at a room temperature. Further, the higher discharge rate, the lower discharge capacity is. Battery discharge capacity fade modeling at different operating conditions is still an ongoing and challenging research direction. In this paper, two new battery discharge capacity fade models have been proposed. In the first model, the relationship between capacity fading and discharge rate is formulated. The other model derives a relation between capacity fading and temperature. The main contributions of this paper are summarized as follows. Firstly, given battery discharge capacity fade data at different discharge rates, a battery capacity fading model is proposed to model a relationship among discharge capacity fading, charge–discharge cycling and discharge rate for a population of batteries. The proposed discharge capacity fading model at different discharge rates is then formulated to a linear and Gaussian state space model so as to use on-line monitoring discharge capacity fading data of a new single operating battery to estimate the posterior parameters of the proposed model for further accurate RUL prediction of a single operating battery. Secondly, given battery discharge capacity fading data at different temperatures, a battery discharge capacity fading model at different temperatures is proposed to model a relationship among discharge capacity fading, charge–discharge cycling and temperature. Then, the proposed model is reformulated as a nonlinear state space model so as to use on-line discharge capacity fading data of a single operating battery to posteriorly update model parameters for achieving accurate RUL of a new single operating battery.

The rest of this paper is outlined as follows. In Section II, battery discharge capacity fade modeling at different discharge rates and its Bayesian updating for a single operating battery are detailed. In Section III, battery discharge capacity fade modeling at different temperatures and its Bayesian updating for a single operating battery are detailed. In Section IV, two case studies of battery prognostics at different discharge rates and different temperatures are provided to illustrate how the proposed two models work and validates the effectiveness of the proposed models. Conclusions are drawn in the final section.

2. Battery discharge capacity fade modeling at different discharge rates and its Bayesian updating for a single operating battery

In this section, firstly, to experimentally investigate the influence of discharge rate on discharge capacity and its fade, continuous battery cycle testing was designed in our laboratory. Our

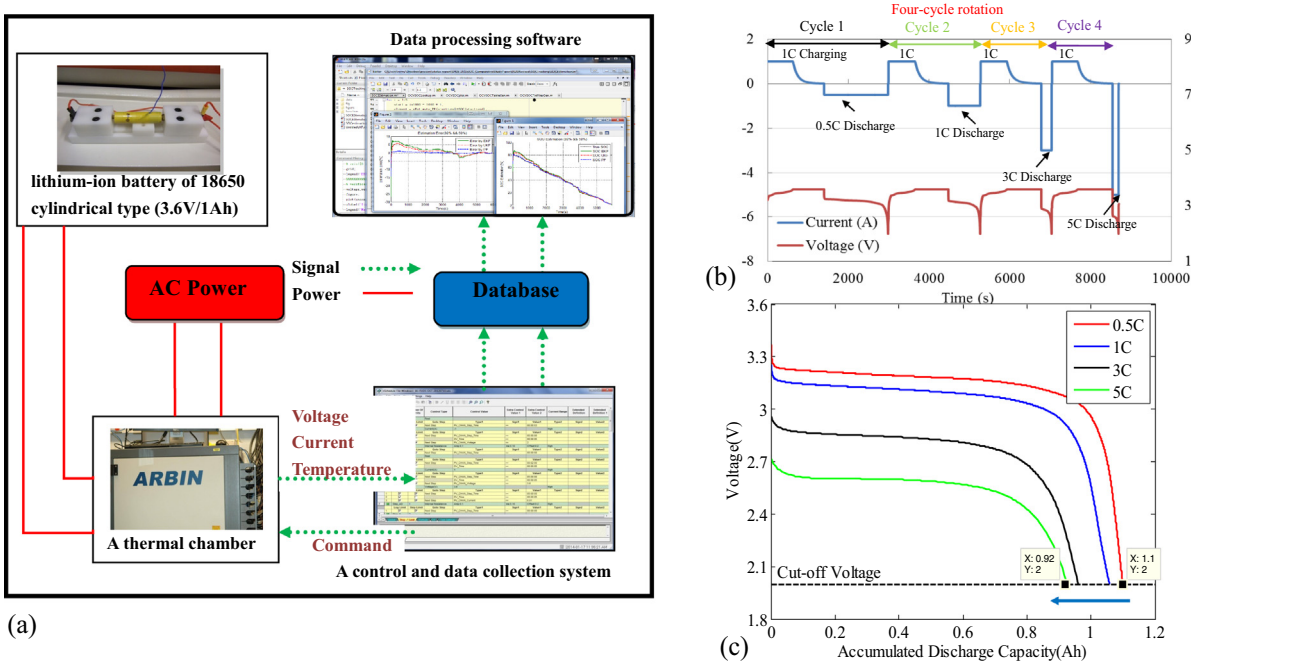

Fig. 1. A four-cycle rotation fading scheme for realizing continuous battery cycle testing at different discharge rates: (a) our experimental platform; (b) a current and voltage profile used in a four-cycle rotation fading scheme (four continuous charge–discharge cycles); (c) a discharge voltage profile in a four-cycle rotation.

experimental platform is shown in Fig. 1, where an Arbin BT2000 tester was used to sample current, voltage and temperature from each of five cylindrical BAK 18650 batteries specified in Table 1 at a constant temperature in a thermal chamber during the continuous battery cycle testing. Because collecting discharge capacity fade data at a low discharge rate, such as 0.5C and 1C, requires much longer time, a four-cycle rotation fading scheme based continuous battery cycle testing was designed to accelerate discharge capacity fade at different discharge rates. Specifically, for each battery, the four-cycle rotation fading scheme contained four continuous charge–discharge cycles. Firstly, a battery was charged at a 1C constant current to reach a voltage of 3.6 V and then the voltage kept fixed until a cutoff current of C/20 was reached. Further, a 0.5C constant current was used to discharge the battery until a cutoff voltage of 2 V was reached. The battery was recharged again and it was discharged at a 1C constant current. Here, constant current charge/discharge modes were used because we followed constant charge/discharge modes commonly used in the literature review to design our own experiments at different operating conditions. The similar procedure was conducted at discharge rates of 3C and 5C, respectively, after the battery was recharged at a 1C constant current. At last, one four-cycle rotation including continuous four charge–discharge cycles was completed. To realize the continuous battery cycle testing, the four-cycle rotation fading scheme was repeated again and again.

Discharge capacity fade of a battery at different discharge rates is plotted in Fig. 2 as an example. The first observation in Fig. 2 is that, given a specific four-cycle rotation (four continuous charge–discharge cycles), discharge capacity at different discharge rates is different. Moreover, the higher a discharge rate, the lower discharge capacity. To investigate a relationship between discharge capacity and discharge rate I, given an arbitrary four-cycle rotation, a linear model $\beta_1 + \beta_2 \times I$ is used to regress discharge capacity at different rates. Here, β_1 and β_2 are the two parameters of the linear model. The fitted coefficients are plotted in Fig. 3(a) and (b),

Table 1
Specifications of BAK 18650 batteries.

Cathode	LiFeO4
Anode	Graphite
Rated capacity	1.1 Ah
C-rate	1.1A
Upper/lower cut-off voltage	3.6 V/2V
End of charge current	0.01C

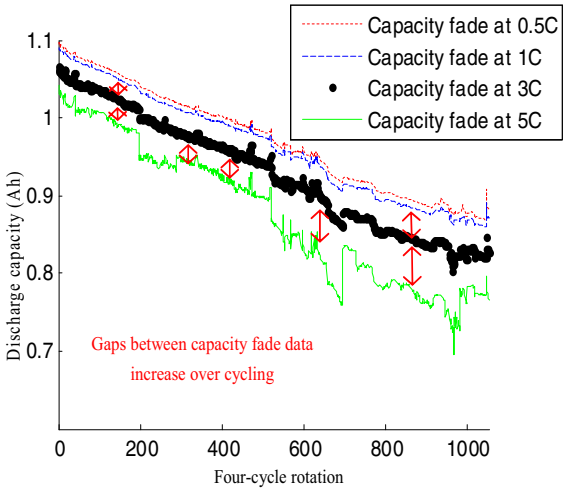

Fig. 2. Discharge capacity fade of a battery at different discharge rates.

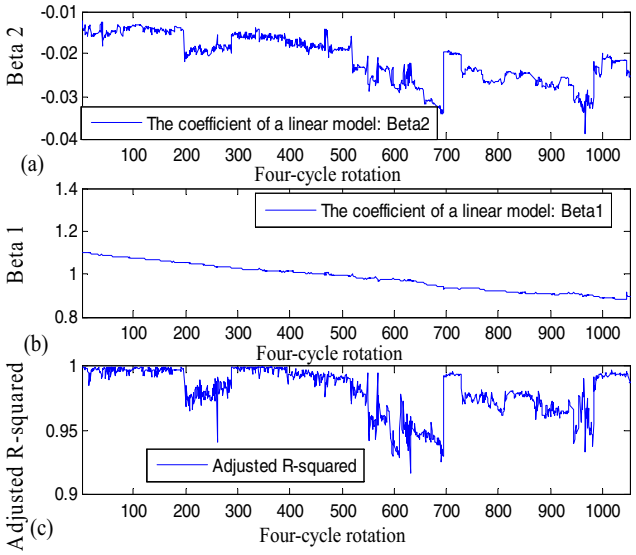

Fig. 3. Results of a linear model $\beta_1 + \beta_2 \times I$ for fitting discharge capacity at different discharge rates and each four-cycle rotation: (a) β_2 over cycling; (b)β_1 over cycling; (c) the adjusted R-squared of the linear model.

respectively, where it is found that β_1 and β_2 are varied over four-cycle rotations and both of them are the function of four-cycle rotations. Further, the adjusted R-square of the linear model in Fig. 3(c) demonstrates that the linear model is sufficiently good to fit discharge capacity at different discharge rates and a four-cycle rotation. The closer the adjusted R-square is to 1, the better the fitting ability of the linear model is. Therefore, according to the results shown in Fig. 3, an initial discharge capacity fade model is formulated as follows:

$$f(k,I) = \beta_1(k) + \beta_2(k) \times I \tag{1}$$

where $f(k,I)$ is discharge capacity at four-cycle rotation k and discharge rate I; $\beta_1(k)$ and $\beta_2(k)$ are the two parameters of the linear model and they are a function of four-cycle rotation k. (1) is consistent with the second observation in Fig. 2 that is the gaps between discharge capacity fade at a discharge rate of 1C and discharge capacity fade at discharge rates of 3C and 5C increase over four-cycle rotations.

On the other hand, given a specific discharge rate, it is not difficult to check that a linear model $a + b \times k$ is sufficiently good to fit discharge fade over four-cycle rotations. The related results are plotted in Fig. 4. Therefore, in (1), $\beta_1(k) = a + b \times k$. If we consider a linear model $\beta_2(k) = c + d \times k$ and zero-mean independent and identically distributed Gaussian noises $\varepsilon(k) \sim N(0, \sigma^2)$ with a variance σ^2, the discharge capacity fade model $f(k,I)$ at different discharge rates is ultimately proposed in this paper as follow:

$$f(k,I) = \lambda_1 + \lambda_2 \times k + \lambda_3 \times I + \lambda_4 \times k \times I + \varepsilon(k) \tag{2}$$

where $\lambda_1, \lambda_2, \lambda_3, \lambda_4$ are the parameters of the proposed model in (2). Here, it is found an interaction item $\lambda_4 \times k \times I$ exists, which is caused by the four-cycle rotation k and the discharge rate I. Then, (2) is used to fit all of the discharge capacity fade data in Fig. 2. The fitted result is plotted in Fig. 5, where the adjusted R-square is equal to 0.9778. The fitting results of the proposed model for processing the discharge capacity fade data of four more batteries at different discharge rates are tabulated in Table 2, where it is indicated that the proposed discharge capacity fade model in (2) is capable of accurately describing discharge capacity fade at different discharge rates. Moreover, because capacity fade is continuously

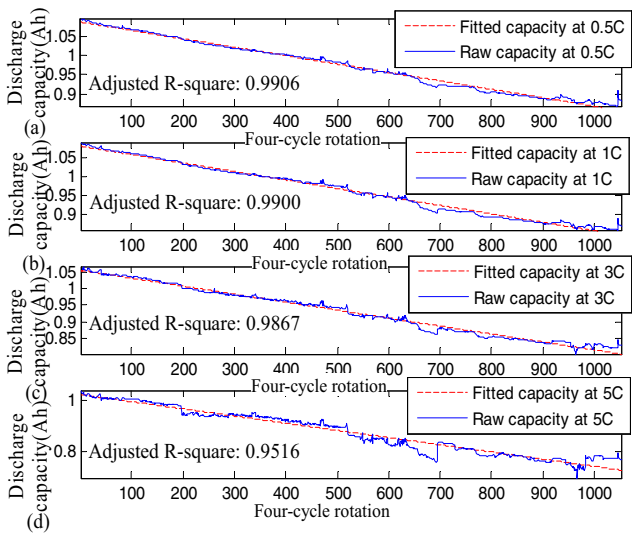

Fig. 4. Fitting results of a linear model $a + b \times k$: (a) at a discharge rate 0.5C; (b) at a discharge rate 1C; (c) at a discharge rate 3C; (d) at a discharge rate 5C.

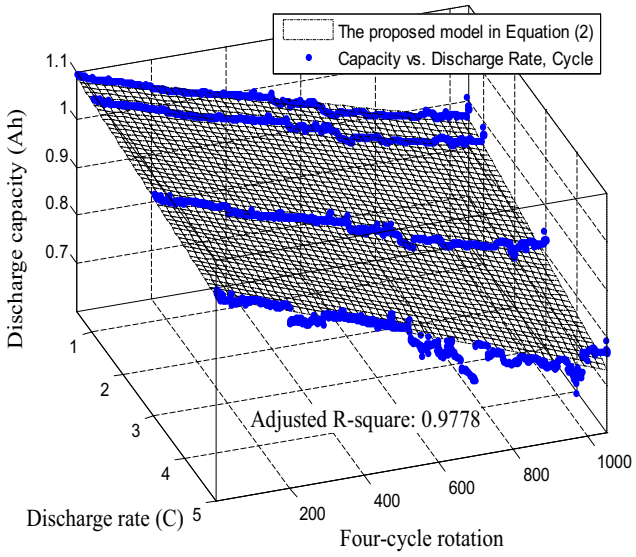

Fig. 5. Result of the proposed fade model in (2) for fitting discharge capacity fade at different discharge rates in Fig. 2.

changed with discharge rate, (2) is a continuous function with respect to discharge rate, which indicates that (2) can work at different discharge rates ranged from 0.5C to 5C. For example, capacity fade at a discharge rate of 2C should be located on the modeling surface in Fig. 5.

To model a unit-to-unit variance and use online discharge capacity data of a single operating battery to posteriorly update the parameters of the proposed model in (2) and predict RUL of a single operating battery more accurately, the proposed model in (2) is transformed to a state space model as follows:

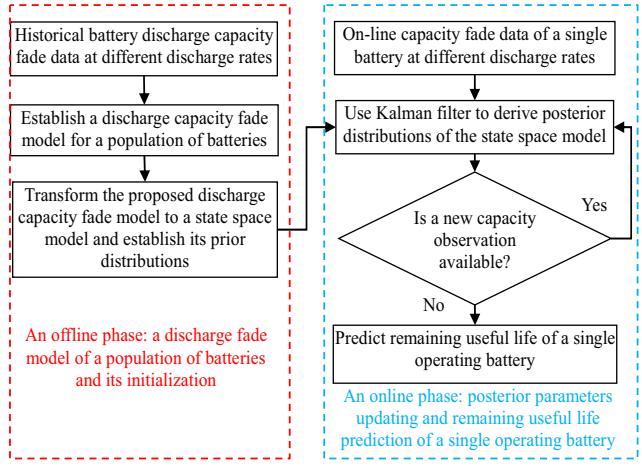

Fig. 6. A flowchart of the proposed discharge capacity fade model for predicting RUL of a single operating battery at different discharge rates.

$$\begin{aligned} \mathbf{x}_k &= \mathbf{x}_{k-1} + \omega_k \\ y_k &= \mathbf{H}_k \mathbf{x}_k + \varepsilon_k \end{aligned} \tag{3}$$

where $\mathbf{x}_k = [\lambda_1 \quad \lambda_2 \quad \lambda_3 \quad \lambda_4]'$ is a parameter vector at four-cycle rotation k; ω_k is zero-mean multivariate Gaussian noises with a covariance $\mathbf{Q}_k$; $\mathbf{H}_k = [1 \quad k \quad I \quad kI]$ is an observation model which is used to map $\mathbf{x}_k$ in a state space into an observed space; y_k is a discharge capacity observation at four-cycle rotation k. Because the state space model in (3) is linear and Gaussian, a Kalman filter [30] is the best choice to recursively update the parameters vector. The Kalman filter has two phases including prediction and update in the following.

3. Prediction phase

Before a new discharge capacity observation y_k at four-cycle rotation k is available, the predicted estimate $\mathbf{x}_{k|k-1}$ of the parameters vector at four-cycle rotation k is $\mathbf{x}_{k-1|k-1}$ and the variance $\mathbf{P}_{k|k-1}$ of the predicted estimate $\mathbf{x}_{k|k-1}$ is $\mathbf{P}_{k|k-1} = \mathbf{P}_{k-1|k-1} + \mathbf{Q}_k$. Here, $\mathbf{x}_{k-1|k-1}$ is the posterior estimate of the parameters vector when observations $y_{1:k-1}$ up to four-cycle rotation $k-1$ are available.

4. Update phase

After a new discharge capacity observation y_k at four-cycle rotation k is available, an observation residual is $y_k - \mathbf{H}_k \mathbf{x}_{k|k-1}$, the posterior estimate $\mathbf{x}_{k|k}$ of the parameters vector at four-cycle rotation k is $\mathbf{x}_{k|k} = \mathbf{x}_{k|k-1} + \mathbf{K}_k (y_k - \mathbf{H}_k \mathbf{x}_{k|k-1})$ and the variance $\mathbf{P}_{k|k}$ of the posterior estimate $\mathbf{x}_{k|k}$ is $\mathbf{P}_{k|k} = \mathbf{P}_{k|k-1} - \mathbf{K}_k \mathbf{H}_k \mathbf{P}_{k|k-1}$. Here, the optimal Kalman filter gain is $\mathbf{K}_k = \mathbf{P}_{k|k-1} \mathbf{H}_k^T \mathbf{S}_k^{-1}$, where the variance of the observation residual $\mathbf{S}_k = \mathbf{H}_k \mathbf{P}_{k|k-1} \mathbf{H}_k^T + \sigma^2$.

Table 2
The fitting results of the proposed model in (2) for processing discharge capacity of four more batteries at different discharge rates.

Battery Number	Adjusted R-square	λ_1	λ_2	λ_3	λ_4
Battery 1	0.9778	1.094	-2.074×10^{-04}	−0.01359	-1.424×10^{-05}
Battery 2	0.9853	1.055	-4.385×10^{-04}	−0.01353	-3.882×10^{-05}
Battery 3	0.9933	1.09	-2.176×10^{-04}	−0.01067	-1.092×10^{-05}
Battery 4	0.9046	1.105	-1.646×10^{-04}	−0.04297	-9.195×10^{-06}
Battery 5	0.9796	1.093	-4.374×10^{-04}	−0.01793	-3.027×10^{-05}

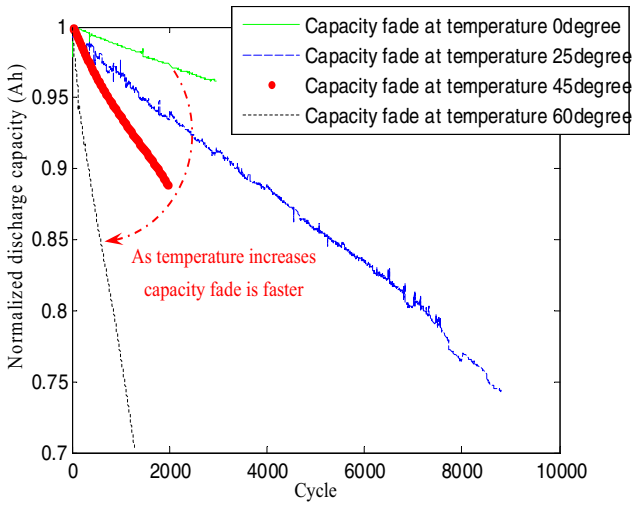

Fig. 7. Normalized discharge capacity fade data of four batteries at different temperatures.

Once the parameters vector is updated at four-cycle rotation k, a discharge capacity observation y_{k+l} at four-cycle rotation $k+l$ follows a Gaussian distribution with a mean μ_{k+l} and a variance σ^2_{k+l} as follows:

$$\mu_{k+l} = \mathbf{H}_{k+l}\mathbf{x}_{k|k} \tag{4}$$

$$\sigma^2_{k+l} = \mathbf{H}_{k+l}\mathbf{P}_{k|k}\mathbf{H}^T_{k+l} + \sigma^2 \tag{5}$$

Given a specific soft failure threshold D and the available observations $y_{1:k}$ up to four-cycle rotation k, the conditional cumulative distribution of battery RUL L at different discharge rates is given as follows:

$$P(L \leqslant l|y_{1:k}) = P(y_{k+l} \leqslant D|y_{1:k}) = P\left(Z \leqslant \frac{D-\mu_{k+l}}{\sigma_{k+l}}\right) = \Phi(f(l)) \tag{6}$$

where Z is the standard Gaussian random variable and its cumulative distribution is $\Phi(\cdot)$; $f(l) = (D-\mu_{k+l})/\sigma_{k+l}$. Because RUL is required to be positive, (6) is revised as:

$$P(L \leqslant l|y_{1:k}, L \geqslant 0) = \frac{P(0 \leqslant L \leqslant l|y_{1:k})}{P(L \geqslant 0|y_{1:k})} = \frac{\Phi(f(l)) - \Phi(f(0))}{1-\Phi(f(0))} \tag{7}$$

The derivative of (7) with respect to l can be derived as:

$$g_{L\leqslant l|y_{1:k}, L\geqslant 0}(l) = \frac{\phi(f(l))f'(l)}{1-\Phi(f(0))} \tag{8}$$

where $\phi(\cdot)$ is the probability density function (PDF) of the standard Gaussian random variable; the derivative of $f(l)$ with respect to l is detailed in Appendix A. At last, the proposed discharge capacity fade model for rechargeable battery prognostics at different discharge rates is summarized in Fig. 6, where an offline phase and an online phase are used. The offline phase aims to construct a discharge capacity fade model at different discharge rates for a population of batteries, while the online phase aims to use monitoring data of a single operating battery to posteriorly update the parameters of the discharge capacity fade model and predict RUL of a single operating battery at different discharge rates.

5. Battery discharge capacity fade modeling at different temperatures and its Bayesian updating for a single operating battery

Based on our experimental platform, to experimentally investigate the influence of different temperatures including 0 °C, 25 °C (room temperature), 45 °C and 60 °C on discharge capacity and its fade, eight A123 APR18650m1A lithium iron phosphate batteries (with datasheets in reference [31]) were recharged at 1C and discharged at 1C, respectively. The normalized discharge capacity fade data of four batteries at the four aforementioned temperatures are plotted in Fig. 7.

The first observation in Fig. 7 is that batteries at different temperatures have different fade rates. The higher a temperature, the faster a battery fades. It is clearly observed that a relationship between temperature T and discharge capacity is nonlinear.

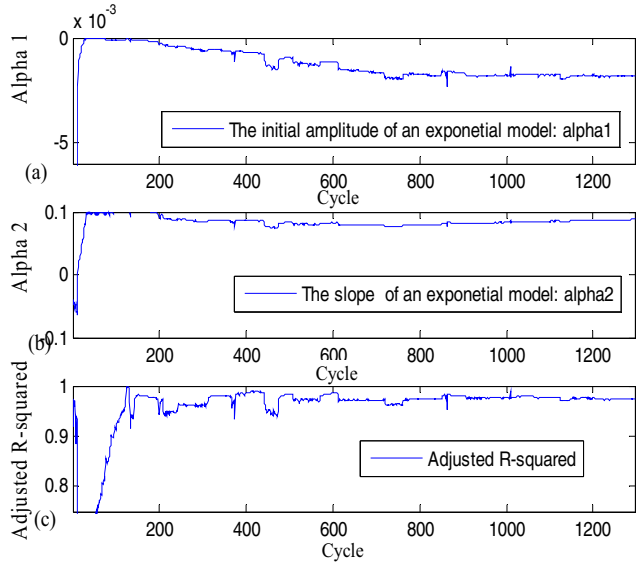

Fig. 8. Results of an exponential model $\alpha_1 \exp(\alpha_2 \times T)$ for fitting the logarithm of discharge capacity at different temperatures: (a) α_1 over cycling; (b)α_2 over cycling; (c) the adjusted R-squared of the exponential model.

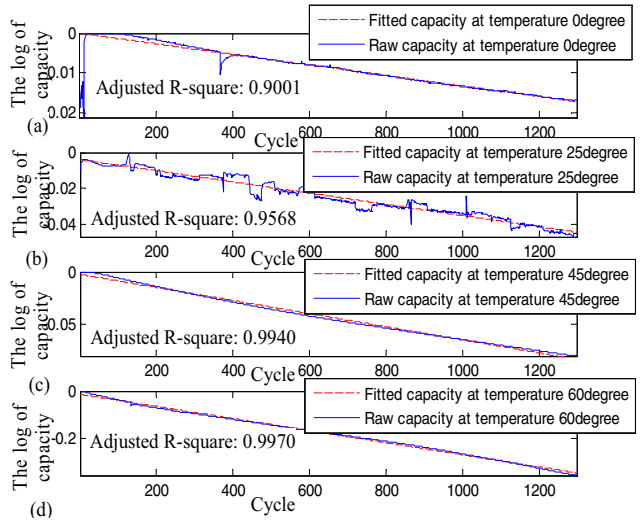

Fig. 9. Fitting results of a linear model $z + x \times n$: (a) at a temperature 0 °C; (b) at a temperature 25 °C; (c) at a temperature 45 °C; (d) at a temperature 60 °C.

According to our analyses, given a cycle, the logarithm of discharge capacity can be well fitted by an exponential model $\alpha_1\exp(\alpha_2 \times T)$. Here, α_1 and α_2 are the initial amplitude and slope of the exponential model, respectively. The fitted parameters are plotted in Fig. 8 (a) and (b), respectively, where it is observed that the initial amplitude of the exponential model seems a linear function of cycles, while the slope of the exponential model tends to a stable level. Further, the adjusted R-square in Fig. 8(c) demonstrates that the exponential model is sufficiently good to fit discharge capacity at different temperatures over cycling. The closer the adjusted R-square is to 1, the better the fitting ability of the exponential model is. Consequently, the relationship between discharge capacity and temperature at a cycle can be written as follows:

$$\ln f_1(n,T) = \alpha_1(n) \times \exp(\alpha_2 \times T) \tag{9}$$

where $\ln f_1(n,T)$ is discharge capacity at a cycle n and temperature T; $\alpha_1(n)$ and α_2 are the two parameters of the exponential model.

On the other hand, given a specific temperature, it is easy to check that a linear model $z + x \times n$ is sufficient to fit capacity discharge fade over cycling. The related results for processing discharge capacity fade at different temperatures are plotted in Fig. 9. If we consider identically distributed Gaussian noises $\varepsilon_1(n) \sim N(0,\sigma_1^2)$ with a variance σ_1^2 and the aforementioned statements, the discharge capacity fade model $f_1(n,T)$ at different temperatures is proposed in this paper as follow:

$$\ln f_1(n,T) = (\eta_1 + \eta_2 n)\exp(\eta_3 T) + \varepsilon_1(n) \tag{10}$$

where η_1, η_2, η_3 are the parameters of the proposed model in (10). Here, $\eta_2 n\exp(\eta_3 T)$ is an interaction item between temperature T and cycle n. Then, (10) is used to fit the discharge capacity fade at different temperatures in Fig. 7 and the fitting result is plotted in Fig. 10, where the adjusted R-square is equal to 0.9844. The fitted parameters are $\eta_1 = -8.73 \times 10^{-5}$, $\eta_2 = -1.666 \times 10^{-6}$ and $\eta_3 = 8.367 \times 10^{-2}$. Moreover, because capacity fade is continuously changed with temperature, (10) is a continuous function with respect to temperature, which indicates that (10) can work at different temperatures ranged from 0 °C to 60 °C.

Further, to model a unit-to-unit variance and use online discharge capacity data of a single operating battery to update the posterior parameters of the proposed model in (10) and predict RUL of a single operating battery, the proposed model in (10) is transformed to a nonlinear and Gaussian state space model as follows:

$$\begin{aligned} \mathbf{z}_n &= \mathbf{z}_{n-1} + v_n \\ \ln y_n &= (\eta_1 + \eta_2 n)\exp(\eta_3 T) + \varepsilon_{1,n} \end{aligned} \tag{11}$$

where $\mathbf{z}_n = [\eta_1 \quad \eta_2 \quad \eta_3]'$ is a parameter vector at cycle n; v_n is zero-mean multivariate Gaussian with a covariance $\mathbf{Q}_n$; $\varepsilon_{1,n}$ is zero-mean Gaussian noises with a variance σ_2^2. Because a nonlinear relationship exists in (11), Kalman filter is unable to provide posterior distributions for the proposed model in (10). In this case, particle filter [32] is a powerful tool to estimate posterior distributions of the proposed model in (10) and its idea is simply introduced as follows. Suppose that the posterior distribution of $\mathbf{z}_{n-1}$ at cycle $n-1$ is available. A number of random particles $\{\mathbf{z}_n^b\}_{b=1}^{N_s}$ are drawn from the posterior distribution of $\mathbf{z}_{n-1}$ and their weights are $\left\{\vartheta_{n-1}^b\right\}_{b=1}^{N_s}$. N_s is the number of random particles. After a new discharge capacity observation y_n at cycle n is available, the weight of each random particle is updated by:

$$\vartheta_n^b \propto \vartheta_{n-1}^b \exp\left(\frac{-\left(\log y_n - (\eta_1^b + \eta_2^b n)\exp(\eta_3^b T)\right)^2}{2\sigma_2^2}\right), b = 1,2,\ldots,N_s \tag{12}$$

Then, normalize all weights. To avoid the degenerative problem of the particle filter, a systematic resampling algorithm [32] is adopted to redraw random particles according to the size of their weights when the condition $\left(\sum_{b=1}^{N_s}\left(\vartheta_{n-1}^b\right)^2\right)^{-1} < 0.9 \times N_s$ is satisfied. The posterior distribution of $\mathbf{z}_n$ at cycle n is expressed by using random particles and their weights:

$$g(\mathbf{z}_n|y_{1:k}) = \sum_{b=1}^{N_s} \vartheta_n^b \delta(\eta_1 - \eta_1^b, \eta_2 - \eta_2^b, \eta_3 - \eta_3^b) \tag{13}$$

Given a specific soft failure threshold D and observations $y_{1:k}$ up to cycle n, the PDF of battery RUL L at different temperatures is given as follows:

$$g(l|y_{1:k}, D) = \sum_{b=1}^{N_s} \vartheta_n^b \delta(l - (\tau - n)) \tag{14}$$

where $\tau = \inf(j \in int : (\eta_1^b + \eta_2^b j)\exp(\eta_3^b T) \leqslant \ln D)$. Finally, the proposed discharge capacity fade model for rechargeable battery prognostics at different temperatures is summarized in Fig. 11, where an offline phase and an online phase are used. The offline phase aims to construct a discharge capacity fade model for a population of

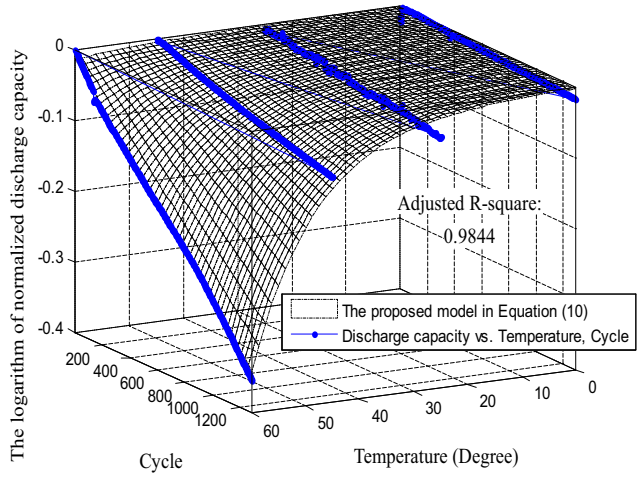

Fig. 10. Result of the proposed model in (10) for fitting discharge capacity fade data at different temperatures in Fig. 7.

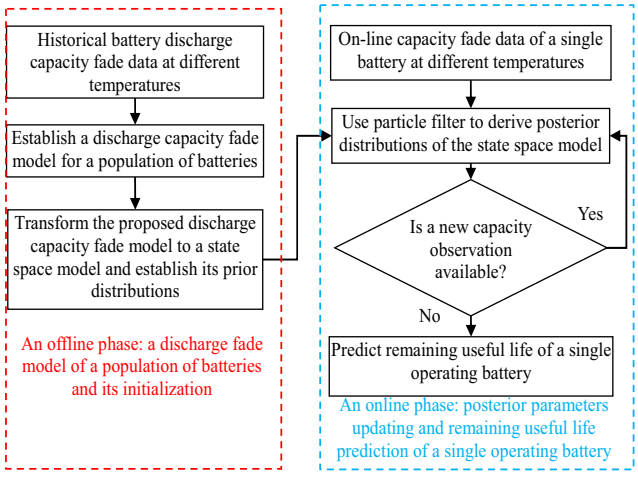

Fig. 11. A flowchart of the proposed discharge capacity fade model for predicting RUL of a single operating battery at different temperatures.

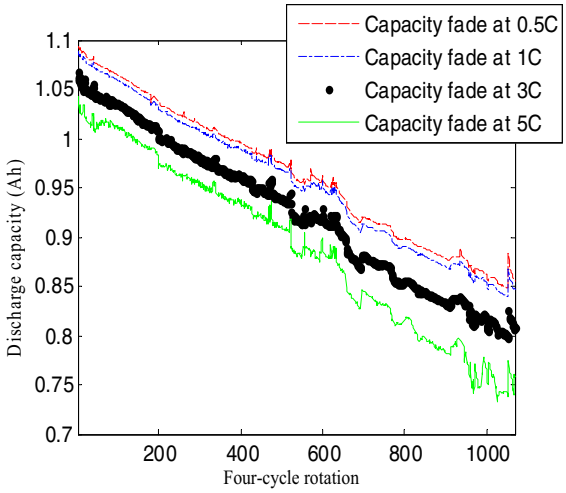

Fig. 12. Discharge capacity fade of a testing battery at different discharge rates.

batteries at different temperatures, while the online phase aims to use monitoring data of a single operating battery to posteriorly update the parameters of the discharge capacity fade model and predict RUL of a single operating battery at different temperatures.

6. Case studies of the proposed discharge capacity fade models for battery prognostics at different discharge rates and different temperatures

In this section, we will illustrate how to use on-line discharge capacity fade data of a new single operating battery to posteriorly update the parameters of the proposed two discharge capacity fade models for predicting RUL of a single operating battery at different discharge rates and different temperatures. Moreover, it should be noted that battery fade datasets used in this section are split into historical datasets and testing datasets. The historical datasets aim to construct the proposed battery fade models for a population of batteries, while the testing datasets aim to use on-line monitoring fade data of a single operating battery to posteriorly update model parameters and predict RUL of a single operating battery. Because at each iteration only one online discharge capacity data of a single operating battery is used to update the posterior parameters of the proposed models in the solid mathematical frameworks of the Kalman filter and the particle filter, the calculation time of posterior parameters estimation is very fast and RUL prediction can be realized in real time.

7. A case study of the proposed discharge capacity fade model for battery prognostics at different discharge rates

In this subsection, we use battery prognostics at different discharge rates as a case study to experimentally demonstrate the effectiveness of the proposed discharge capacity fade model at different discharge rates. Five sets of battery capacity fade data at different discharge rates in the continuous battery cycle testing in Section II are randomly divided as a historical dataset and a testing dataset. The historical dataset is relevant to a population of four batteries, which have a common degradation trend proposed in (2), and then the historical dataset is used to initialize the proposed state space model formulated in (3), which is used to model a unit-to-unit variance according to the idea of the dynamic Bayesian inference/Kalman filter. The testing dataset in Fig. 12 is further utilized to illustrate how the proposed discharge capacity fade model is posteriorly updated and how battery RUL at different discharge

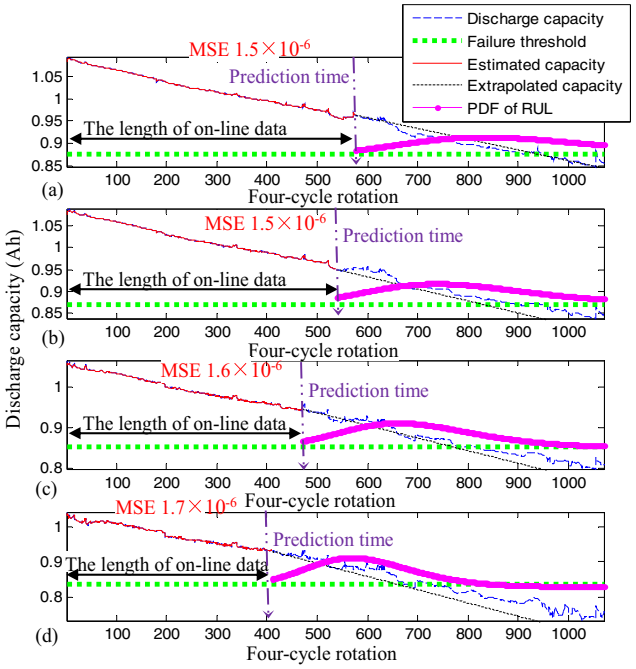

Fig. 13. Visualization of battery prognostic results at different discharge rates: (a) prognostic results at a discharge rate 0.5C; (b) prognostic results at a discharge rate 1C; (c) prognostic results at a discharge rate 3C; (d) prognostic results at a discharge rate 5C.

rates is predicted when a new online discharge capacity observation of a single operating battery is available. The initialization of the proposed model can be easily realized by taking the average and variance of the fitted parameters tabulated in Table 2. The initial parameter vector is equal to $\mathbf{x}_0 = \begin{bmatrix} 1.0867 & -3.1198\times10^{-4} & -2.2\times10^{-2} & -2.3131\times10^{5} \end{bmatrix}'$. The initial covariance $\mathbf{Q}_k$ is equal to a diagonal matrix $\begin{bmatrix} 4.7758\times10^{-4} & 0 & 0 & 0 \\ 0 & 2.1465\times10^{-8} & 0 & 0 \\ 0 & 0 & 1.9959\times10^{-4} & 0 \\ 0 & 0 & 0 & 1.9012\times10^{-10} \end{bmatrix}$, which indicates that the four parameters are assumed to be independent of each other at the very beginning before Bayesian inference is conducted by using the Kalman filter. The variance of observation noises is taken as the variance of the residuals obtained by fitting the historical battery fade data with the proposed model at different discharge rates in (2) and it is equal to 2.5986×10^{-4}. Besides, the mean of the same residuals is equal to 3.0568×10^{-11}, which indicates that the assumption of a zero mean holds on. After the proposed discharge capacity model at different discharge rates is initialized, on-line capacity fade data of a single operating battery can be used to posteriorly update the initial parameters of the proposed model for modeling particular battery capacity fade over cycling.

For example, modeling the testing battery fade at different discharge rates at a specific prediction time is visualized in Fig. 13, where it is observed that the estimated discharge capacity in the red line accurately tracks the true discharge capacity because mean squared errors (MSEs) between estimated capacity and true capacity are very small. Here, a prediction time can be defined as a percent of actual battery lifetime at a specific discharge rate and the actual lifetime is regarded as the first hitting time of a battery at a specific discharge rate when its discharge capacity falls below a failure threshold, such as 80 percent of initial capacity at a specific discharge rate, for the first time. Due to the influence of different discharge rates on discharge capacity, four different failure thresh-

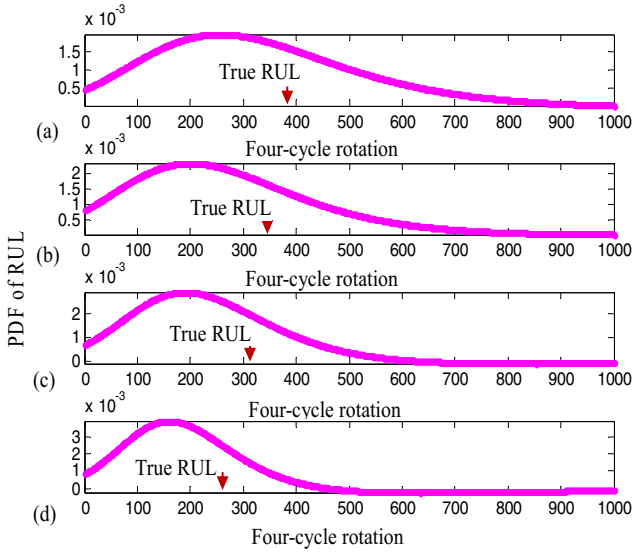

Fig. 14. PDFs of RUL in Fig. 13 at different discharge rates: (a) PDF of RUL at a discharge rate 0.5C; (b) PDF of RUL at a discharge rate 1C; (c) PDF of RUL at a discharge rate 3C; (d) PDF of RUL at a discharge rate 5C.

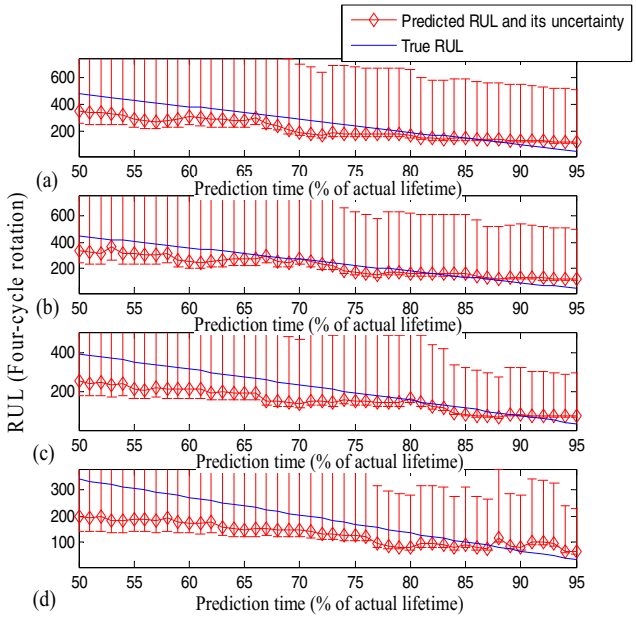

Fig. 15. Comparisons of predicted RUL and true RUL for battery prognostics at different discharge rates: (a) at a discharge rate 0.5C; (b) at a discharge rate 1C; (c) at a discharge rate 3C; (d) at a discharge rate 5C.

olds are used in Fig. 13(a)–(d), respectively. Further, once the latest available discharge capacity is used to posteriorly update the parameters of the proposed model, extrapolations of the proposed model to reaching the failure thresholds are used to infer battery RUL and its uncertainty. The PDFs of RUL at different discharge rates in Fig. 13 are zoomed in Fig. 14. More RUL prediction results at different discharge rates and prediction times are diagramed in Fig. 15, where it is observed that the proposed prognostic capacity fade model can predict RUL accurately. Here, prediction errors are the difference between true RUL and predicted RUL. For example, in Fig. 15, prediction errors are the difference between true RUL and predicted RUL highlighted by the diamond at different prediction times. Moreover, when more online discharge capacity data of a single operating battery are available, the RUL prediction accuracies at different discharge rates become more accurate.

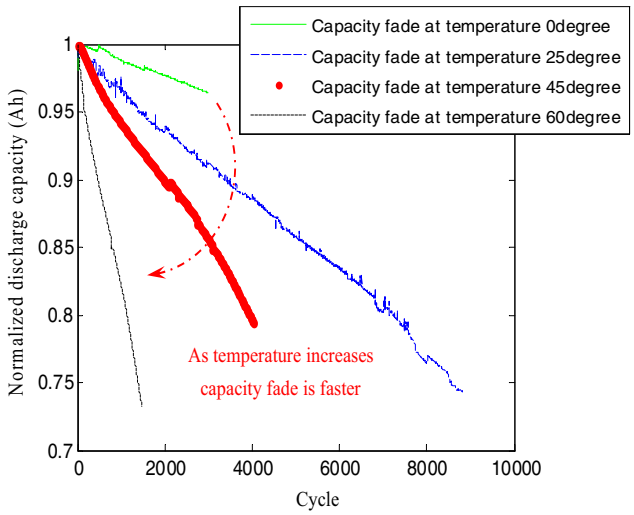

Fig. 16. Normalized discharge capacity fade of four testing batteries at different temperatures.

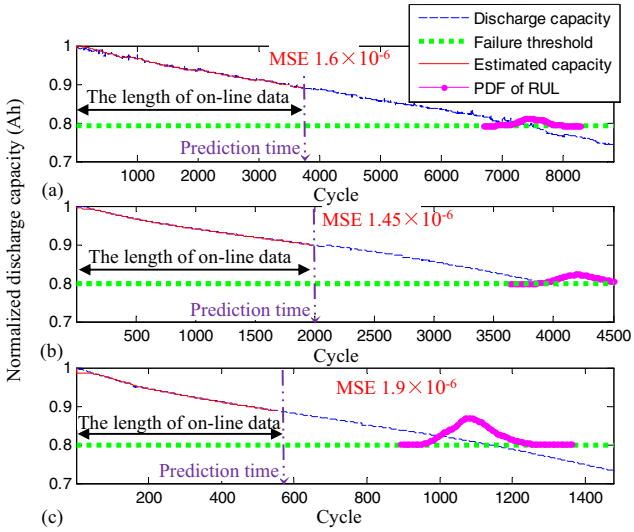

Fig. 17. Visualization of battery prognostic results at different temperatures: (a) prognostic results at a temperature of 25 °C; (b) prognostic results at a temperature of 45 °C; (c) prognostic results at a temperature of 60 °C.

8. A case study of the proposed discharge capacity fade model for battery prognostics at different temperatures

In this section, we use battery prognostics at different temperatures as a case study to experimentally demonstrate the effectiveness of the proposed discharge capacity fade model at different temperatures. Collecting battery discharge capacity fade data at different temperatures is very time-consuming because different temperatures have different influences on discharge capacity fade. The battery discharge capacity fade data shown in Fig. 7 are used as historical data, which are provided by the continuous cycling test of the four batteries at different temperatures. Three new battery degradation fade data at temperatures 0 °C, 45 °C and 60 °C are used as a testing dataset and they are plotted in Fig. 16. Firstly, it is necessary to initialize the proposed model. The initial parameter vector is equal to $\mathbf{z}_0 = \left[-8.73\times10^{-5}\ \ -1.666\times10^{-6}\ \ 8.367\times10^{-2}\right]'$. Since we do not have sufficient battery discharge capacity fade data at different temperatures, the initial variance $\mathbf{Q}_n$ of the

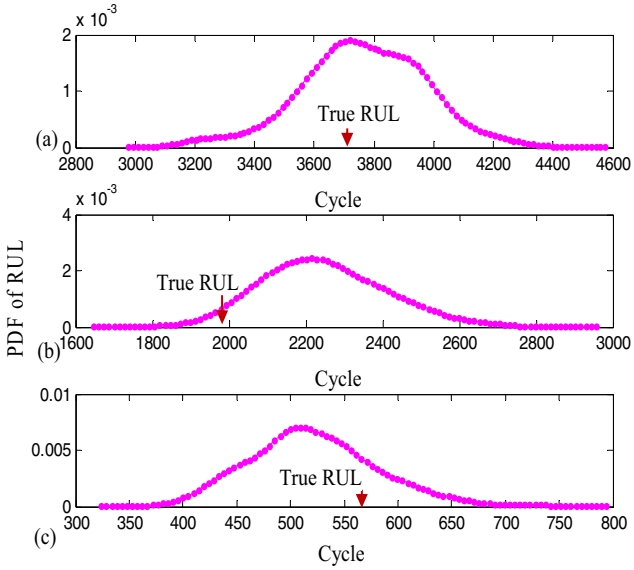

Fig. 18. PDFs of RUL in Fig. 17 at different temperatures: (a) prognostic results at a temperature 25 °C; (b) prognostic results at a temperature 45 °C; (c) prognostic results at a 60 °C.

zero-mean multivariate Gaussian noises is calculating by considering the sixth (the six sigma principle) of the 95% confidence bounds of the parameter estimates of the proposed model in (10), which can be easily realized by the nonlinear regression analysis, and the multivariate Gaussian variance is equal to $\begin{bmatrix} 2.63\times10^{-6} & 0 & 0 \\ 0 & 2.08\times10^{-8} & 0 \\ 0 & 0 & 2.08\times10^{-4} \end{bmatrix}$. The variance of observation noises is taken as the variance of the residuals obtained by fitting the historical battery fade data with the proposed model at different temperatures in (10) and it is equal to 9×10^{-3}. Being similar with the previous section, once new online capacity observations of a single operating battery are available, the new data can be used to posteriorly update the initial parameters of the proposed model and model a unit-to-unit variance. For example, the results provided by using the proposed battery prognostic model at different temperatures are visualized in Fig. 17, where it is observed that the estimated discharge capacity in the red line is accurate to track the true capacity since MSEs between estimated capacity and true capacity are very small. Moreover, after the posterior parameters of the proposed model are established, extrapolations of the determined model to reaching the failure threshold can be used to infer the PDF of RUL of a single operating battery, which are zoomed in Fig. 18. More RUL prediction results at different prediction times and different temperatures are plotted in Fig. 19, where it is observed that the proposed model can predict the true RUL accurately and the RUL prediction accuracies become more accurate when more and more on-line discharge capacity fade data are available.

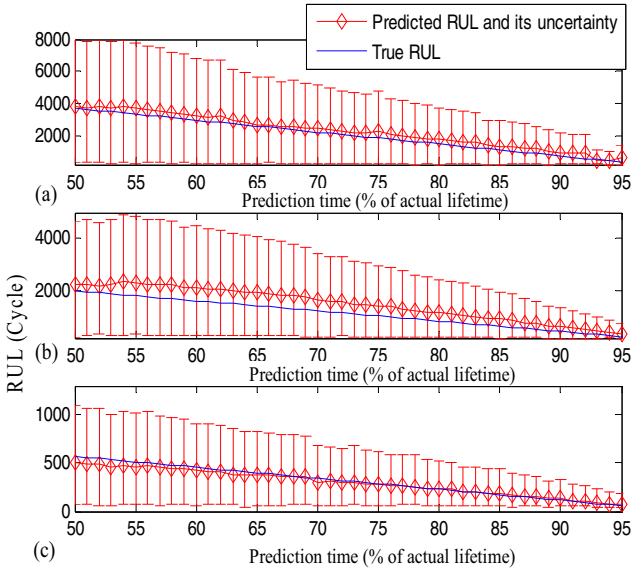

Fig. 19. Comparisons of predicted RUL and true RUL for battery prognostics at different temperatures: (a) prognostic results at a temperature 25 °C; (b) prognostic results at a temperature 45 °C; (c) prognostic results at a 60 °C.

9. Conclusion

In this paper, to model battery discharge capacity fade at different discharge rates and different temperatures, we proposed two discharge capacity models for a population of batteries in (2) and (10), respectively. Because these two models aimed to model a population of rechargeable batteries at different discharge rates and different temperatures, both of them can not accurately describe single operating battery fade at a specific discharge rate or a specific temperature. To model a unit-to-unit variance, two state space models were respectively proposed in (3) and (11) and then the parameters of these two state space models were posteriorly updated when new online observations of a single operating battery were available. At last, two battery case studies were conducted to experimentally demonstrate the effectiveness of the proposed capacity fade models at different discharge rates and different temperatures. The results showed that the proposed model can track the true capacity fade data well and predict the true RUL of a single operating battery accurately.

Declaration of Competing Interest

The authors declare that they have no known competing financial interests or personal relationships that could have appeared to influence the work reported in this paper.

Acknowledgements

This research work is supported by National Natural Science Foundation of China (Grant No. 51975355 and Grant No. 71901188), the General Research Fund (Project No. CityU 11206417), the Research Grants Council Theme-based Research Scheme under Project T32-101/15-R, and Research Impact Fund (Project No. R5020-18). The authors would like to thank three reviewers for their constructive and valuable comments.

Appendix A

In (4) and (5), it is shown that an observation y_{k+l} at four-cycle rotation $k+l$ follows a Gaussian distribution with a mean μ_{k+l} and a variance σ^2_{k+l}. We can calculate the mean μ_{k+l} and its derivative with respect to l as follows:

$$\begin{aligned} \mu_{k+l} &= \mathbf{H}_k\mathbf{x}_{k|k} = [1 \quad (k+l) \quad I \quad (k+l)I]\left[x_{1,k|k} \quad x_{2,k|k} \quad x_{3,k|k} \quad x_{4,k|k}\right]' \\ &= x^1_{k|k} + (k+l)x_{2,k|k} + Ix_{3,k|k} + (k+l)\times Ix_{4,k|k} \\ \Rightarrow \quad & \mu'_{k+l} = x_{2,k|k} + Ix_{4,k|k} \end{aligned} \tag{15}$$

We can calculate the variance σ^2_{k+l} and the derivative of its square root with respect to l as follows:

$$
\begin{aligned}
\sigma_{k+l}^2 = \;& \mathbf{H}_{k+l}\mathbf{P}_{k|k}\mathbf{H}_{k+l}^T + \sigma^2 \\
= \;& \begin{bmatrix} 1 & k+l & I & (k+l)I \end{bmatrix} \begin{bmatrix} P_{k|k}^{11} & P_{k|k}^{12} & P_{k|k}^{13} & P_{k|k}^{14} \\ P_{k|k}^{21} & P_{k|k}^{22} & P_{k|k}^{23} & P_{k|k}^{24} \\ P_{k|k}^{31} & P_{k|k}^{32} & P_{k|k}^{33} & P_{k|k}^{34} \\ P_{k|k}^{41} & P_{k|k}^{42} & P_{k|k}^{43} & P_{k|k}^{44} \end{bmatrix} \begin{bmatrix} 1 \\ k+l \\ I \\ (k+l)I \end{bmatrix} + \sigma^2 \\
= \;& P_{k|k}^{11} + P_{k|k}^{21}(k+l) + P_{k|k}^{31}I + P_{k|k}^{41}(k+l)I \\
+ \;& \left(P_{k|k}^{12} + P_{k|k}^{22}(k+l) + P_{k|k}^{32}I + P_{k|k}^{42}(k+l)I\right)(k+l) \\
+ \;& \left(P_{k|k}^{13} + P_{k|k}^{23}(k+l) + P_{k|k}^{33}I + P_{k|k}^{43}(k+l)I\right)I \\
+ \;& \left(P_{k|k}^{14} + P_{k|k}^{24}(k+l) + P_{k|k}^{34}I + P_{k|k}^{44}(k+l)I\right)(k+l)I + \sigma^2 \\
= \;& \left(P_{k|k}^{11} + 2P_{k|k}^{31}I + P_{k|k}^{33}I^2\right) + \left(2P_{k|k}^{21} + 2P_{k|k}^{41}I + 2P_{k|k}^{32}I + 2P_{k|k}^{43}I^2\right)(k+l) \\
+ \;& \left(P_{k|k}^{22} + 2P_{k|k}^{42}I + P_{k|k}^{44}I^2\right)(k+l)^2 + \sigma^2 \\
\Rightarrow \;& \sigma'_{k+l} = \left(\sigma_{k+l}^2\right)^{-\frac{1}{2}} \begin{pmatrix} \left(P_{k|k}^{21} + P_{k|k}^{41}I + P_{k|k}^{32}I + P_{k|k}^{43}I^2\right) \\ +2\left(P_{k|k}^{22} + 2P_{k|k}^{42}I + P_{k|k}^{44}I^2\right)(k+l) \end{pmatrix}
\end{aligned} \tag{16}
$$

Finally, the derivative of $f(l)$ with respect to l is given as follows:

$$
\begin{aligned}
f'(l) = \;& \left(\frac{D-\mu_{k+l}}{\sigma_{k+l}}\right)' = \frac{\left(D-\mu_{k+l}\right)'\sigma_{k+l} - \left(D-\mu_{k+l}\right)\sigma'_{k+l}}{\sigma_{k+l}^2} \\
= \;& \frac{-\mu'_{k+l}\sigma_{k+l} - \left(D-\mu_{k+l}\right)\sigma'_{k+l}}{\sigma_{k+l}^2}
\end{aligned} \tag{17}
$$

References

[1] P. Ralon, M. Taylor, A. Ilas, H. Diaz-Bone, K. Kairies, Electricity Storage and Renewables: Costs and markets to 2030, United Arab Emirates, International Renewable Energy Agency, Abu Dhabi, 2017.

[2] M. Pecht, Prognostics and Health Management of Electronics, 1st ed., Wiley-Interscience, London, 2008.

[3] J. Zhang, J. Lee, A review on prognostics and health monitoring of Li-ion battery, J. Power Sour. 196 (15) (2011) 6007–6014.

[4] Z.S. Ye, M. Xie, Stochastic modelling and analysis of degradation for highly reliable products, Appl. Stochastic Models Bus. Ind. 31 (1) (2015) 16–32.

[5] Z. Zhang, X. Si, C. Hu, Y. Lei, Degradation data analysis and remaining useful life estimation: a review on wiener-process-based methods, Eur. J. Oper. Res. (2018).

[6] M.A. Hannan, M. Lipu, A. Hussain, A. Mohamed, A review of lithium-ion battery state of charge estimation and management system in electric vehicle applications: challenges and recommendations, Renew. Sustain. Energy Rev. 78 (2017) 834–854.

[7] M.U. Ali, A. Zafar, S.H. Nengroo, S. Hussain, M.J. Alvi, H.-J. Kim, Towards a smarter battery management system for electric vehicle applications: a critical review of lithium-ion battery state of charge estimation, Energies 12 (3) (2019) 446.

[8] F. Yang, Y. Xing, D. Wang, K.-L. Tsui, A comparative study of three model-based algorithms for estimating state-of-charge of lithium-ion batteries under a new combined dynamic loading profile, Appl. Energy 164 (2016) 387–399.

[9] Z. Wei, C. Zou, F. Leng, B.H. Soong, K. Tseng, Online model identification and state-of-charge estimate for lithium-ion battery with a recursive total least squares-based observer, IEEE Trans. Ind. Electron. 65 (2) (2018) 1336–1346.

[10] M.U. Ali, M.A. Kamran, P.S. Kumar, S.H. Himanshu, M.A. Nengroo, A. Khan, H.-J Kim Hussain, An online data-driven model identification and adaptive state of charge estimation approach for lithium-ion-batteries using the lagrange multiplier method, Energies 11 (11) (2018) 2940.

[11] S. Liu, J. Wang, Q. Liu, J. Tang, H. Liu, Z. Fang, Deep-discharging li-ion battery state of charge estimation using a partial adaptive forgetting factors least square method, IEEE Access 7 (2019) 47339–47352.

[12] K. Goebel, M. Daigle, S. Abhinav, S. Sankararaman, I. Roychoudhury, J. Celaya, Sci. Mak. Predictions (2017).

[13] B. Saha, K. Goebel, S. Poll, J. Christophersen, Prognostics methods for battery health monitoring using a bayesian framework, Instrum. Meas. IEEE Trans. 58 (2) (2009) 291–296.

[14] B. Saha, K. Goebel, J. Christophersen, Comparison of prognostic algorithms for estimating remaining useful life of batteries, Trans. Inst. Meas. Control 31 (3–4) (2009) 293–308.

[15] W. He, N. Williard, M. Osterman, M. Pecht, Prognostics of lithium-ion batteries based on dempster-Shafer theory and the Bayesian Monte Carlo method, J. Power Sour. 196 (2011) 10314–10321.

[16] Y. Xing, E.W. Ma, K.-L. Tsui, M. Pecht, An ensemble model for predicting the remaining useful performance of lithium-ion batteries, Microelectron. Reliabil. 53 (6) (2013) 811–820.

[17] F. Yang, D. Wang, Y. Xing, K.-L. Tsui, Prognostics of Li (NiMnCo) O 2-based lithium-ion batteries using a novel battery degradation model, Microelectron. Reliab. 70 (2017) 70–78.

[18] J. Yu, State-of-health monitoring and prediction of lithium-ion battery using probabilistic indication and state-space model, IEEE Trans. Instrum. Meas. 64 (11) (2015) 2937–2949.

[19] Q. Miao, L. Xie, H. Cui, W. Liang, M. Pecht, Remaining useful life prediction of lithium-ion battery with unscented particle filter technique, Microelectron. Reliab. 53 (6) (2013) 805–810.

[20] C. Hu, G. Jain, P. Tamirisa, T. Gorka, Method for estimating capacity and predicting remaining useful life of lithium-ion battery, Appl. Energy 126 (2014) 182–189.

[21] D. Wang, F. Yang, K.-L. Tsui, Q. Zhou, S.J. Bae, Remaining useful life prediction of lithium-ion batteries based on spherical cubature particle filter, Instrument. Meas. IEEE Trans. 65 (6) (2016) 1282–1291.

[22] M. Jouin, R. Gouriveau, D. Hissel, M.-C. Péra, N. Zerhouni, Particle filter-based prognostics: review, discussion and perspectives, Mech. Syst. Signal Pr. 72 (2016) 2–31.

[23] X. Xu, Z. Li, N. Chen, A hierarchical model for lithium-ion battery degradation prediction, IEEE Trans. Reliab. 65 (1) (2016) 310–325.

[24] B.E. Olivares, M.A. Cerda Munoz, M.E. Orchard, J.F. Silva, Particle-filtering-based prognosis framework for energy storage devices with a statistical characterization of state-of-health regeneration phenomena, instrumentation and measurement, IEEE Trans. 62 (2) (2013) 364–376.

[25] Z.-X. Zhang, X.-S. Si, C.-H. Hu, M.G. Pecht, A Prognostic model for stochastic degrading systems with state recovery: application to li-ion batteries, IEEE Trans. Reliab. 66 (4) (2017) 1293–1308.

[26] D. Liu, W. Xie, H. Liao, Y. Peng, An integrated probabilistic approach to lithium-ion battery remaining useful life estimation, IEEE Trans. Instrum. Meas. 64 (3) (2015) 660–670.

[27] X.-S. Si, An adaptive prognostic approach via nonlinear degradation modeling: application to battery data, IEEE Trans. Ind. Electron. 62 (8) (2015) 5082–5096.

[28] D. Wang, K.-L. Tsui, Brownian motion with adaptive drift for remaining useful life prediction: revisited, Mech. Syst. Signal Pr. 99 (2018) 691–701.

[29] J. Vetter, P. Novák, M. Wagner, C. Veit, K.-C. Möller, J. Besenhard, M. Winter, M. Wohlfahrt-Mehrens, C. Vogler, A. Hammouche, Ageing mechanisms in lithium-ion batteries, J. Power Sour. 147 (1–2) (2005) 269–281.

[30] G. Bishop, G. Welch, An introduction to the Kalman filter, Proc of SIGGRAPH, Course 8(27599-23175) (2001) 41.

[31] A123 APR18650m1A cell. https://www.batteryspace.com/prod-specs/6612.pdf.

[32] M.S. Arulampalam, S. Maskell, N. Gordon, T. Clapp, A tutorial on particle filters for online nonlinear/non-Gaussian Bayesian tracking, IEEE Trans. Signal Process. 50 (2) (2002) 174–188.